Cell, Vol. 121, 257–270, April 22, 2005, Copyright ©2005 by Elsevier Inc. DOI 10.1016/j.cell.2005.02.005

Structures of MLS_BK Antibiotics Bound to Mutated Large Ribosomal Subunits Provide a Structural Explanation for Resistance

Daqi Tu,[1,4,5] Gregor Blaha,[1,4] Peter B. Moore,[1,2] and Thomas A. Steitz[1,2,3,*]

[1]Department of Molecular Biophysics and Biochemistry

[2]Department of Chemistry

Yale University

[3]Howard Hughes Medical Institute

New Haven, Connecticut 06520

Summary

Crystal structures of *H. marismortui* large ribosomal subunits containing the mutation G2099A (A2058 in *E. coli*) with erythromycin, azithromycin, clindamycin, virginiamycin S, and telithromycin bound explain why eubacterial ribosomes containing the mutation A2058G are resistant to them. Azithromycin binds almost identically to both G2099A and wild-type subunits, but the erythromycin affinity increases by more than 10^4-fold, implying that desolvation of the N2 of G2099 accounts for the low wild-type affinity for macrolides. All macrolides bind similarly to the *H. marismortui* subunit, but their binding differs significantly from what has been reported in the *D. radioidurans* subunit. The synergy in the binding of streptogramins A and B appears to result from a reorientation of the base of A2103 (A2062, *E. coli*) that stacks between them. The structure of large subunit containing a three residue deletion mutant of L22 shows a change in the L22 structure and exit tunnel shape that illuminates its macrolide resistance phenotype.

Introduction

Many clinically important antibiotics specifically inhibit the activity of eubacterial ribosomes, and prominent among them are the macrolide, lincosamide, streptogramin B, and ketolide antibiotics, which are often called the MLS_BK antibiotics. All members of this chemically heterogeneous group bind to the peptidyl transferase center of the large ribosomal subunit at sites that are close to each other or overlapping (Spahn and Prescott, 1996), and bacterial strains resistant to any one of them tend to be resistant to all.

Bacterial strains resistant to MLS_BK antibiotics commonly contain either an N-methyl transferase that methylates the exocyclic N6 amine of A2058 (*E. coli* numbering) in 23S rRNA or a mutated 23S rRNA, often A2058G (Weisblum, 1995). Resistance mutations also occur in the loops of ribosomal proteins L4 and L22, which come close together in the wall of the peptide exit tunnel, not far from where MLS_BK antibiotics bind (Chittum and Champney, 1994; Malbruny et al., 2002; Wittmann et al., 1973).

In the last two years, crystal structures have been published for several MLS_BK antibiotics bound to the large ribosomal subunits. Yonath and coworkers have obtained structures of *Deinococcus radiodurans* (Dra) large ribosomal subunit complexed with erythromycin and telithromycin, which are 14-membered macrolides, a lincosamide, clindamycin, and dalfopristin and quinupristin, which are streptogramins of the A and B types, respectively (Berisio et al., 2003; Harms et al., 2004; Schlünzen et al., 2001). The structures of the 15-membered macrolide, azithromycin, the 16-membered macrolides, carbomycin A, spiramycin, and tylosin, and finally virginiamycin M, which is an A-type streptogramin, bound to the large ribosomal subunit from *Haloarcula marismortui* (Hma) have also been determined (Hansen et al., 2002a; Hansen et al., 2003). While the locations of the MLS_BK antibiotic binding sites on the ribosomes from both species are grossly similar, there are surprising differences in detail. The conformations of many of these antibiotics as well as their interactions with the surrounding ribosomal structure are in many cases strikingly different.

One possible explanation for the differences in the models of the MLS_BK antibiotics bound to the ribosomes of the two species Hma and Dra is that Hma, like most archaebacteria, has a G at position 2058, but Dra, like most eubacteria, has an A at that position. In eubacteria, A2058G mutations confer resistance to MLS_BK antibiotics, and as expected, Hma ribosomes are resistant to them (Sanz et al., 1993). Indeed, a crystalline complex of erythromycin bound to the Dra large subunit has been obtained using a drug concentration of 0.1 mM (Schlünzen et al., 2001), whereas erythromycin does not bind to crystals of Hma large subunits even at a concentration of 3 mM (J.L. Hansen, P.B.M., and T.A.S., unpublished data).

In order to determine whether or not the A/G difference at position 2058 accounts for the structural differences reported, we have determined the structures of several MLS_BK antibiotic complexes with Hma large subunits containing mutations that should affect their sensitivity to these drugs. Mutant ribosomes were obtained from several different strains of Hma carrying rRNA operons in which the 23S rRNA gene of *rrnA* cistron is mutated from G to A at position 2058 and from a strain in which the gene for L22 has the three amino acid deletion that in *E. coli* reduces sensitivity to macrolides without reducing their affinity for the ribosome. The erythromycin affinity of Hma large subunits containing the G2058A mutation is about 10^4 times higher than that of wild-type, and using this mutated Hma large ribosomal subunit, its crystal structure with erythromycin bound has been obtained. We have also determined the structures of this mutated large ribosomal subunit bound to telithromycin, azithromycin, clindamycin, quinupristin, and virginiamycin M and S together, which are streptogramins of the A and B types, respectively.

*Correspondence: eatherton@csb.yale.edu

[4]These authors contributed equally to this work.

[5]Present address: Department of Molecular and Cellular Physiology, Stanford University, Stanford, California 94305.

Table 1. Crystallographic Statistics

Data Collection							
Crystal	Antibiotic	Res (Å)[a]	I/σ[b]	R_{merge}[c]	Complete[d]	Red[d]	λ[e]
50% G2099A	Erythromycin	50.0–2.65 (2.74–2.65)	24.4 (1.9)	7.0 (71)	99.2 (94.0)	6.3	1.10
33% G2099A	Telithromycin	50.0–2.60 (2.69–2.60)	22.5 (1.8)	7.8 (80)	99.0 (91.9)	6.5	1.10
100% G2099A	Azithromycin	50.0–2.40 (2.49–2.40)	22.6 (1.8)	6.2 (71)	95.7 (72.1)	4.8	1.10
33% G2099A	Virginiamycin M + S	50.0–2.85 (2.95–2.85)	15.5 (2.2)	8.2 (59)	99.8 (99.9)	3.5	1.10
33% G2099A	Clindamycin	50.0–3.00 (3.11–3.00)	11.2 (1.8)	10.8 (67)	98.2 (96.6)	4.1	1.10
100% G2099A	Quinupristin	50.0–3.00 (3.11–3.00)	9.4 (1.9)	13.2 (62)	91.1 (92.6)	4.7	1.10
L22(Δ3aa)	—	50.0–2.90 (3.00–2.90)	10.4 (2.0)	9.1 (60)	97.2 (97.2)	3.0	1.08

Model Refinement								
Crystal	Antibiotic	Res (Å)[a]	I/σ[b]	R_{cryst}[f]	R_{free}[g]	Bond[h]	Ang[h]	B[i]
50% G2099A	Erythromycin	30.0–2.65 (2.74–2.65)	(1.9)	17.7	21.4	0.005	1.0	75
33% G2099A	Telithromycin	30.0–2.60 (2.69–2.60)	(1.8)	18.2	21.9	0.005	1.0	65
100% G2099A	Azithromycin	30.0–2.40 (2.49–2.40)	(1.8)	19.0	22.9	0.005	1.0	37
33% G2099A	Virginiamycin M+S	30.0–2.80 (2.90–2.80)	(1.7)	17.4	22.1	0.005	1.0	35, 42
33% G2099A	Clindamycin	30.0–3.00 (3.11–3.00)	(1.8)	17.0	22.8	0.005	1.0	57
100% G2099A	Quinupristin	30.0–2.90 (3.00–2.90)	(1.1)	17.0	22.3	0.005	1.0	55
L22(Δ3aa)	—	30.0–2.80 (2.90–2.80)	(1.4)	18.5	24.3	0.006	1.1	

[a] Resolution range for X-ray diffraction data followed in parenthesis by resolution range of high-resolution bin.
[b] I/σ, intensity/error.
[c] $R_{merge} = \{\Sigma_{hkl}\Sigma_i|I_i(hkl) - i(hkl)|\}/\{\Sigma_{hkl}\Sigma_i[I_i(hkl)]\}$, where i(hkl) is the average intensity of reflection (hkl), and $I_i(hkl)$ is the ith observation.
[d] Complete, completeness of data; Red, redundancy of data.
[e] Wavelength of X-rays in Å.
[f] $R_{cryst} = \{\Sigma_{hkl}|F_c(hkl) - F_o(hkl)|\}/\{\Sigma_{hkl}[F_o(hkl)]\}$, for data used in refinement, where $F_c(hkl)$ is the calculated model-based amplitude for reflection hkl and F_o is the measured amplitude.
[g] Calculated the same as R_{cryst} for a test reflection set which was excluded from all refinement.
[h] Bond and Ang, RMS deviations from standard bond lengths in Å, and bond angles in degrees.
[i] B factor in $Å^2$ refined for all bound antibiotics while setting their occupancy to one.

Even though the G2058A mutation greatly increases the affinity of Hma ribosomes for macrolides, the location and conformation of the macrolide rings bound to these ribosomes are only slightly different from those bound to wild-type large subunits from the same organism (Hansen et al., 2002a) and thus still differ markedly from those reported for macrolide complexes with the Dra subunit (Berisio et al., 2003; Schlünzen et al., 2001). Thus, the differences in the models reported for macrolide antibiotics bound to Hma and Dra cannot be attributed to the sequence difference at position 2058.

The conformation of L22 containing the deletion that causes resistance differs from its conformation in wild-type large ribosomal subunits. The loop of L22 bends away from the tunnel wall, widening the gap between L22 and L4, but no structural change is observed in the region where erythromycin binds. These observations rationalize the chemical protection data reported earlier for such mutants in *E. coli* (Gregory and Dahlberg, 1999) but provide only hints as to why these ribosomes are less sensitive to inhibition by erythromycin. (Unless otherwise stated, in the text that follows, nucleotide or protein residue numbering will refer to Hma, not *E. coli*, but the equivalent number in *E. coli* will be given in parentheses.)

Results

The Preparation of Large Ribosomal Subunit Crystals Containing G2099A 23S rRNA

Using a modified version of a gene replacement system developed for *Halobacterium halobium* (Krebs et al., 1993) and sequence information about *H. marismortui* (Hma) posted on the web by the DasSarma group ([http://zdna2.umbi.umd.edu], Hma contigs version 2), strains of Hma were produced that contain either mutated 23S rRNA genes or a mutated L22 gene (D.T., G.B., P.B.M., and T.A.S., unpublished data). In many of these experiments, G2099A large subunits were prepared from a strain containing two native rRNA operons and a single mutant rRNA operon, and hence the ratio of large subunits containing the G2099A mutation to wild-type large subunits was ~1:2. A few experiments were done using large ribosomal subunits prepared from strains in which the ratio of mutant to wild-type 23S rRNA cistrons was either ~1:1, or only a single, mutated 23S rRNA cistron was present. Southern blots and DNA sequencing of polymerase chain reaction products confirmed the presence of the expected number of rRNA operons in each strain and the identities of the bases at position 2099. RNA sequencing demonstrated that A2099 and G2099 containing 23S rRNA cistrons are produced in strains containing both kinds of genes. The large ribosomal subunits obtained from these strains crystallize under the same conditions as wild-type Hma large ribosomal subunits to produce isomorphous crystals (Ban et al., 2000).

The Structure of Erythromycin Bound to G2099A Large Ribosomal Subunits from Hma

The highest resolution structure of a G2099A large subunit with erythromycin bound was obtained from a crystal containing 50% mutant subunits that had been soaked with 1 mM erythromycin (Table 1). An unbiased

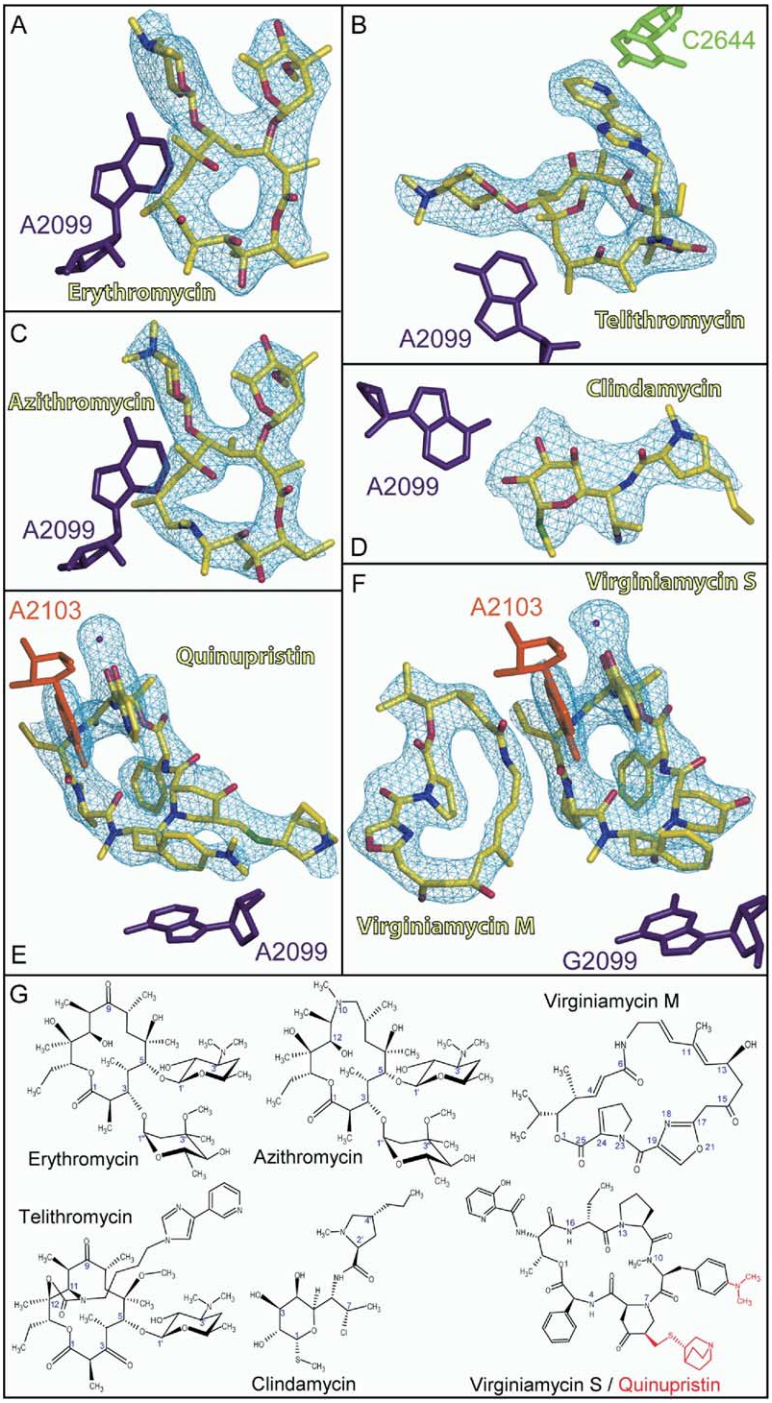

Figure 1. Electron Density Maps of MLS_BK Drugs Bound to G2099A Large Ribosomal Subunits

(A)–(F) are unbiased difference electron density maps computed using (F_o(mutant + drug) – F_o(wild-type – drug)) differences as amplitudes and wild-type phases, which show the position and conformation of: (A) erythromycin at a resolution of 2.75 Å, (B) telithromycin at 2.75 Å, (C) azithromycin at 2.40 Å, (D) clindamycin at 3.00 Å, (E) quinupristin at 3.00 Å, and (F) virginiamycin M and S together at 2.85 Å. The reoriented base of A2103 is included in (E) and (F). The contour level of the electron density is 3.5 σ in (A), (B), and (D), 4.5 σ in (C) and (E), and 6 σ in (F). The resolutions of the erythromycin and telithromycin difference maps shown were determined by the resolution of the isomorphous native data set used, which was lower than that of the drug/ribosome data sets obtained (Table 1).

(G) Chemical structures of erythromycin, telithromycin, azithromycin, clindamycin, virginiamycin S/quinupristin and virginiamycin M.

(F_o (mutant + drug) – F_o (wild-type – drug)) difference electron density map calculated at 2.75 Å resolution using data from this crystal (Figure 1A) clearly showed the conformation and orientation of the bound drug.

Erythromycin lies on the floor of nascent peptide tunnel with the edges of its two sugars pointing toward the ribosomal A and P sites. The 2′OH of its desosamine sugar forms a hydrogen bond with the N1 of A2099 (2058). The side of its lactone ring facing the lumen of the tunnel is hydrophilic. It includes two axially oriented hydroxyl and two axially oriented carbonyl oxygens. In contrast, the face of the lactone ring that contacts the tunnel wall is hydrophobic. It contains no hydrogen bond donors or acceptors, but it does include three methyl groups that insert into the hydrophobic pocket formed by base of A2100 (A2059), the hydrophobic, C2 edge of A2099 (A2058), and the base and sugar of G2646 (C2611) (Figure 2C). The snug fit of this face of erythromycin with the tunnel wall would be altered both sterically and chemically by addition of a hydrophilic

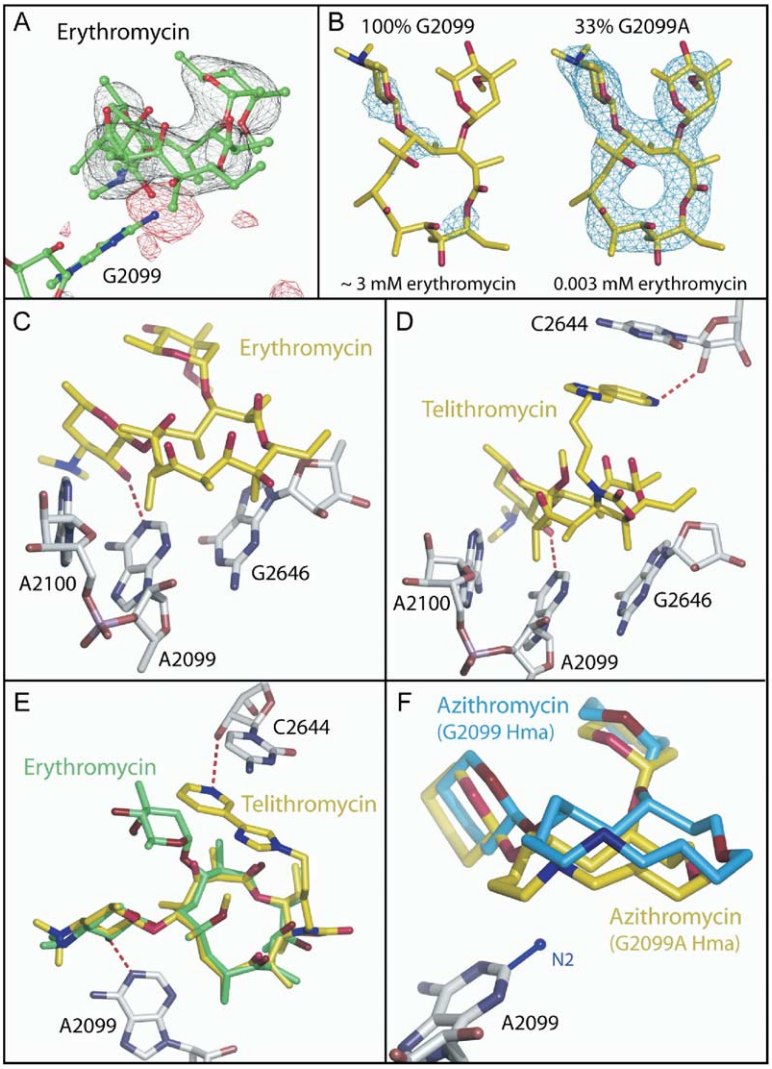

Figure 2. Interactions of Macrolides with G2099A Large Ribosomal Subunits

(A) A (F_o(mutant + drug) – F_o(wild-type – drug)) difference map calculated using wild-type phases shows positive 4 σ density (black) for erythromycin and a negative 4 σ peak (red) at N2 of G2099.

(B) No convincing difference density is observed when erythromycin is soaked into wild-type *H. marismortui* 50S crystal with ~3 mM concentration (left), but when it is soaked into 50S crystals containing 33% G2099A mutants, clear density is observed when the drug concentration is 3 μM (right).

(C) Erythromycin binds in the hydrophobic pocket formed by residue A2100 (A2059), A2099 (A2058), and G2646 (C2611), with its desosamine oxygen hydrogen bonded to A2099N1.

(D) Telithromycin binds in the hydrophobic pocket formed by residue A2100, A2099, and G2646 the way erythromycin does, with its alkyl-aryl extension making an additional stacking interaction with the base of C2644 (U2609) and a hydrogen bond to the 2′OH of C2644 (U2609) .

(E) The lactone rings of erythromycin and telithromycin bound to Hma ribosomes are perfectly superimposable.

(F) Comparison of azithromycin bound to G2099 (blue) and G2099A (yellow) ribosomes. The N2 of a G was modeled onto residue A2099. The two structures compared were aligned by least squares superimposition of ribosomal RNA phosphorus atoms.

group to this part of the tunnel wall, e.g., the N2 of a G at position 2099 (2058).

The presence of the G2099A subunits in these crystals is clearly evident in difference electron density maps. Figure 2A shows the relevant portion of an unbiased difference electron density map calculated using (F_o(mutant + drug) – F_o (wild-type – drug)) amplitudes and wild-type, apo phases. The mutant crystals used contained ~33% G2099A large subunits and were highly isomorphous to the wild-type crystals to which they are compared. In addition to positive electron density for erythromycin, this map includes a negative 4 σ peak at the position occupied by the N2 of G2099 in the wild-type large subunit (Figure 2A), proving that the nucleotide at position 2099 is an A in the mutant large subunits.

A lower-bound estimate of the change in the binding affinity of the Hma large ribosomal subunit for erythromycin afforded by the G2099A mutation was obtained by a crystallographic titration. Erythromycin was soaked into crystals containing 33% G2099A subunits at concentrations of 30 μM, 3 μM, 1 μM, and 0.3 μM. Difference Fourier maps were computed between the observed amplitude data obtained from crystals containing erythromycin at each of these concentrations and native data sets. To determine the concentration at which the occupancy of the drug began to diminish, difference Fourier maps were also calculated between data sets from crystals containing different drug concentrations. Since crystals used in this titration experiment were all from the same batch of subunits, it was not necessary to establish the exact fraction of mutant subunits; it was the same in all crystals.

While the difference map between crystals of wild-type subunit soaked in 3 mM erythromycin and native showed no convincing difference density, the corresponding map using data from the 33% G2099A crystal soaked in 3 μM erythromycin showed full density for the bound drug at a contour level of 3.5 σ (Figure 2B). The same native data set was used for calculating both difference maps, and the cross-R factors between each of the two data sets from the crystals soaked in drug and the same native data set are essentially identical. Thus, the contour levels of the two difference maps should correspond.

Analysis of data from the whole titration series re-

vealed that the erythromycin dissociation constant of G2099A large subunits from Hma is at least 10^4 times smaller than that of wild-type. Difference Fourier maps computed between amplitudes obtained from crystals soaked in 3 μM and 30 μM had no peaks, which means that the occupancy of the erythromycin site is the same in crystals soaked with the drug at those concentrations. However, while the electron density for the drug in difference maps calculated using (F_o(1 μM erythromycin complex) – F_o(native)) amplitudes was clear, the contour level had to be lowered to 2.5 σ, and the difference map calculated between data obtained from crystals soaked in 1 μM erythromycin and those soaked in 3 μM erythromycin showed negative density for the drug. Thus, as the erythromycin concentration drops from 3 μM to 1 μM, its occupancy in these crystals drops appreciably. The dissociation constant, however, could be significantly below 1 μM, since it is possible, indeed likely, that at 1 μM and below occupancy was limited by diffusion. Since erythromycin binding to wild-type Hma large ribosomal subunit is barely detectable at ~3 mM but its binding to G2099A subunits can be detected below 1 μM, difference between the dissociation constants of wild-type and G2099A mutant subunits is at least 10^4.

The Structures of Other Antibiotics Bound to the Mutated Large Subunit

Azithromycin

A structure of azithromycin, a 15-membered macrolide derived from erythromycin, bound to 100% G2099A Hma ribosomes at a resolution of 2.40 Å (Table 1) showed that the two drugs bind to the ribosome in almost exactly the same way (compare Figure 1C with Figure 1A; see also Figure S2 in the Supplemental Data available with this article online).

Telithromycin

Telithromycin is a semisynthetic derivative of erythromycin in which the cladinose sugar linked to C3 of the lactone ring of erythromycin is replaced by a keto group, the hydroxyl group at C6 is methylated, and the C11/C12 position is extended by a carbamate N substituted with an alkyl chain that ends in two aromatic heterocycles. We have established the structure of telithromycin bound to 33% G2099A crystals (Figure 1B) at a resolution of 2.60 Å (Table 1). It binds to G2099A mutant ribosomes in almost exactly the same way as erythromycin. Its lactone ring and desosamine sugar superimpose on those of erythromycin almost perfectly (Figure 2E). The differences in ribosome interactions between the two drugs reflect differences in their lactone ring derivatization. Telithromycin's alkyl-aryl C11/C12 substituent folds across the drug's lactone ring so that its pyridine group stacks on the base of C2644 (U2609) (Figures 2D and S3).

Clindamycin

Clindamycin is a semisynthetic derivative of lincomycin that is used for treatment of diseases caused by gram-positive organisms. The structure of clindamycin bound to G2099A large ribosomal subunits has been determined at a resolution of 3.00 Å (Table 1). The portion of the unbiased ((F_o(mutant + drug) – F_o(wild-type - drug)) difference map that includes the drug is shown in Figure 1D.

Clindamycin binds to the floor of the peptide tunnel in an elongated conformation, with its long axis more or less parallel to the axis of the exit tunnel. Its propyl pyrrolidinyl group occupies the same cleft as the O-methyl tyrosine residue of the A-site substrate CC-puromycin (Hansen et al., 2002b), and the binding site of its galactose group overlaps with the site occupied by the desosamine sugar of macrolides. Clindamycin is oriented and its binding stabilized by hydrogen bonds with rRNA (Figure 3A). The 2OH of its galactose moiety hydrogen bonds to the N1 of A2099, and 3OH forms hydrogen bonds with the N6 of A2099 and the nonbridging phosphate oxygen of G2540 (G2505). In addition, the 4OH of its galactose moiety hydrogen bonds to the 2′OH of A2538 (A2503) and N6 of A2100 (A2059), and the nitrogen atom of the peptide bond linking its galactose moiety to its pyrrolidine group forms a hydrogen bond with the 2′OH of G2540 (G2505).

Virginiamycin M and S

Virginiamycin M and S (a.k.a. streptogramin A and B) are chemically unrelated, macrocyclic lactone peptolides that are produced simultaneously by *Streptomyces virginiae* and synergistically inhibit the growth of gram-positive bacteria (Cocito, 1979). We have solved the structure of virginiamycin M and S bound to the large subunit at a resolution 2.85 Å from a crystal containing 33% G2099A mutant ribosomes that had been soaked with a saturating concentration of a natural virginiamycin mixture containing about 100 μM of S and 600 μM of M (Table 1). A portion of the unbiased electron density map calculated at 2.85 Å resolution using amplitudes ((F_o(mutant + drug) – F_o(wild-type – drug)) show the drugs bind adjacent to each other with the reoriented base of A2103 stacked between them (Figure 1F).

In G2099A ribosomes, virginiamycin M binds at the beginning of the peptide exit tunnel at a site that overlaps those occupied by both A- and P-site substrates, as it does in wild-type Hma large ribosomal subunits (Hansen et al., 2003). Its largely hydrophobic macrocyclic lactone ring fits tightly over hydrophobic base planes of A2486 (A2451) and G2102 (G2061). Its C2 isopropyl group is inserted underneath the base of U2620 (U2585), forming a favorable stacking interaction, and its hydroxyl group at C13 forms a hydrogen bond with the 3′ oxygen of A2538 (A2503). The conjugated amide group (C6/N7) of its lactone ring occupies the position that A2103 (A2062) normally assumes, causing its base to rotate away from the tunnel wall by about 90° into the tunnel lumen. This enables the conjugated amide group of the M component to stack on base of A2103, and its carbonyl oxygen to form a hydrogen bond with 2′OH of A2103 (Figure 3B). The same movement of A2103 was observed when virginiamycin M binds to the wild-type large subunit (Hansen et al., 2003).

Virginiamycin S, which binds adjacent to virginiamycin M in a site that is further down the exit tunnel and is partially supported by its interactions with the M component, occupies space in the lumen of the tunnel. In its overall conformation, virginiamycin S looks like a cup, with its phenyl and pyrrolidine rings stacked on each other to form the bottom of the cup. The hydrophobic edges of those rings stack on the base of U2645 (C2610).

The repositioning of the base of A2103 appears to be

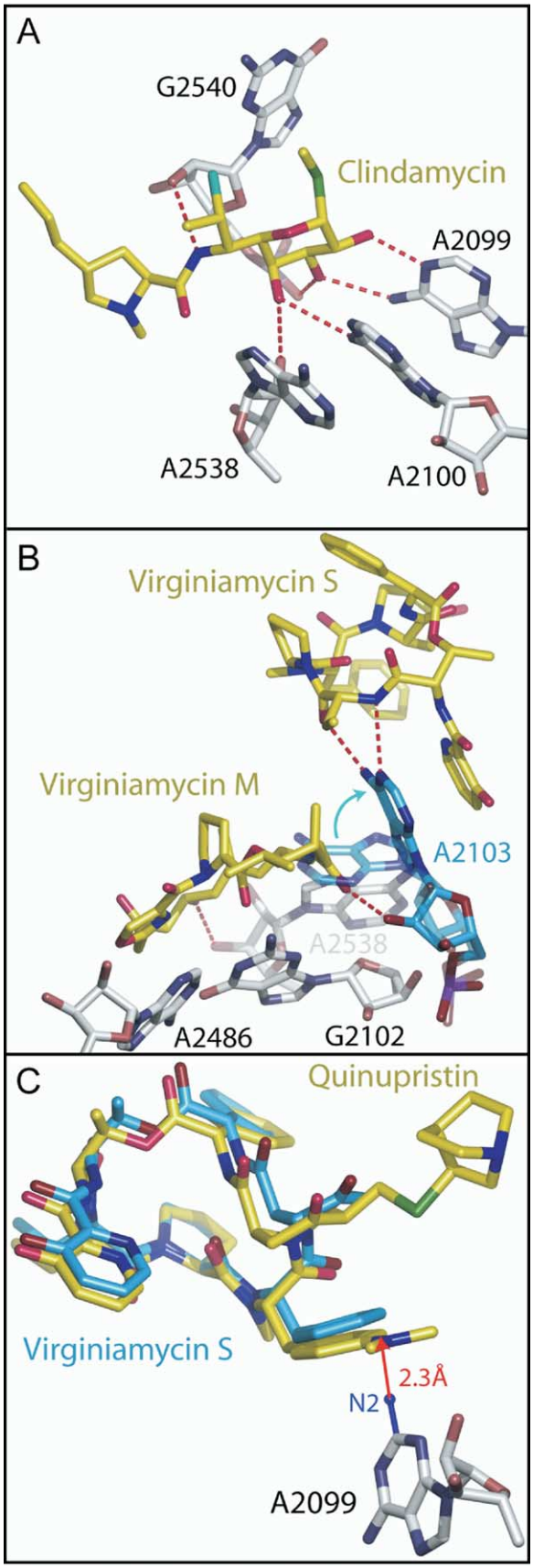

a prerequisite for high affinity binding of virginiamycin S to the ribosome. The repositioned base not only serves as a platform on which the conjugated [(3-hydroxy-2-pyridinyl)carbonyl] amino group from C18 of virginiamycin S can stack, it also brings the N6 and N1 of A2103 close enough to the C14 carbonyl oxygen and the N16 amide nitrogen to enable two hydrogen bonds, respectively (Figure 3B). It is presumably the stacking of this reorientated A on virginiamycin S that results in the cooperative binding observed between these two components.

The S component also makes some hydrophobic contacts with the ribosome. The phenyl residue in C3 of the virginiamycin S lactone ring stacks onto the ribose moiety of C2644 (U2609) and thereby displaces its base by about 45° compared to the native structure of the large subunit. An additional stacking interaction is observed between the aliphatic stretch of C17 to C19 onto the base of pseudouridine 2621 (U2586).

Binding of virginiamycin S to the large subunit is also stabilized by metal ion interactions. A magnesium ion coordinates the hydroxyl and carbonyl oxygens of the conjugated [(3-hydroxy-2-pyridinyl)carbonyl] amino group from C18 of the drug. The octahedral coordination of this magnesium ion is completed by four additional water molecules of which one is in hydrogen bond distance to a nonbridging phosphate oxygen of C2476.

The Effect of G2099A Mutations on Virginiamycin S Binding

The occupancies of the virginiamycin M and S sites in these mixed mutant and wild-type crystals are about the same, which implies that under these conditions, it makes no difference whether large subunits have an A or a G at position 2099. This was not entirely unexpected because in *E. coli*, A2058U mutants do not bind virginiamycin S, but in the presence of virginiamycin M, high-affinity binding of virginiamycin S occurs (Vannuffel et al., 1992). Knowing virginiamycin S binds to both the G2099 or A2099 50S subunit in the presence of virginiamycin M, residue 2099 was modeled as a G during refinement. The N2 of G2099 in the refined structure is 3.0 Å from the closest atom in the C9 benzyl group of virginiamycin S. This juxtaposition should destabilize the binding of virginiamycin S and may explain why A2058G (*E. coli*) mutation confers streptogramin B resistance.

Binding of Virginiamycin S Alone

To gain further insights into the influence of virginiamycin M on virginiamycin S binding, a saturating con-

Figure 3. Interactions of Other MLS_BK Drugs with G2099A Large Ribosomal Subunits

(A) Clindamycin interacts with rRNA through an extensive hydrogen bond network. N6 of A2099 acts as an obligatory hydrogen bond donor to 3OH of the galactose moiety of clindamycin.

(B) Binding of virginiamycin M (VM) to the large subunit causes the base of A2103 to reorient so it can stack on the C18 pyridinyl group of virginiamycin S (VS), thus forming a binding pocket for VS.

(C) Comparison of quinupristin bound to G2099A ribosomes and virginiamycin S bound to G2099 ribosomes as part of virginiamycin M + S pair. N2 of a G was modeled onto residue A2099 and is 2.3 Å from the nearest atom in quinupristin.

centration (~300 μM) of the virginiamycin S derivative quinupristin was soaked into crystals of 100% G2099A large ribosomal subunits. An unbiased ((F_o (mutant + drug) – F_o (wild-type – drug)) difference map at 3.00 Å resolution shows that quinupristin binds at about the same position as that of virginiamycin S in the structure of the complex containing both virginiamycin components (Figure 1E). The base of A2103 adopts the same position that it does when both virginiamycin M and S bind (Figure 1E). This suggests that the reorientation of A2103 caused by the M component completes the binding pocket for the S component, thereby reducing the energy cost of binding of the S component.

The position occupied by quinupristin in these complexes is almost identical to that occupied by virginiamycin S when both virginiamycin components are present (Figure 3C). In addition to slight differences in ring atom positions that are probably not significant experimentally, the C9 dimenthyl amino benzyl group of quinupristin is somewhat closer to residue 2099 than the corresponding group of virginiamycin S, a finding which supports the hypothesis that the benzyl group at C9 of streptogramin B-type drugs clash sterically with the N2 of Gs in position 2099. Resistance to streptogramin B caused by the methylation of the N6 of A2099 (2058) could result from a rotation of the modified base toward the position of the C9 benzyl group caused by a need to increase the contribution of the methylated amine in stacking.

The Structure of the Large Subunit Containing an L22 Mutant

The three amino acid deletion (122–124) in L22 of Hma is equivalent to the deletion mutation in *E. coli* that removes Met82, Lys83, and Arg84 from the conserved C-terminal β hairpin of L22 from *E. coli* and confers erythromycin resistance to *E. coli* ribosomes without reducing their affinity for the drug (Chittum and Champney, 1994; Wittmann et al., 1973). The structure of large subunits containing this mutation was solved at a resolution of 2.90 Å (Table 1).

The three residue deletion from Hma L22 causes its entire C-terminal β hairpin to move away from its normal interaction with the RNA of the tunnel wall, near the erythromycin site, and lodge in the lumen of the peptide exit tunnel closer to its exit (Figure 4C). A difference Fourier map calculated using (F_o(L22Δ3aa) – F_o(native)) as coefficients and contoured at +2.5 σ showed the new position of the L22 loop, which is now bent away from its former orientation by approximately 90° (Figure 4B). Trace density was seen nearby, which suggests that another conformation of the loop is possible in this region, but it was not well enough connected to be modeled.

The same difference Fourier map contoured at –6 σ indicated not only that the 19 residue β hairpin of L22 is not in its normal position but also that three nearby rRNA residues change location (Figure 4A): A1689 (A1614), A841(G748), and U840(U747). Residue U840 moves the furthest and in the mutant fills a location that is normally occupied by the tip of L22 β hairpin. However, the difference electron density also indicated the existence of another conformation for U840, implying this residue is mobile in the absence of the L22 hairpin. A structure of a tylosin complex with these L22 mutant ribosomes shows tylosin binds as previously observed for wild-type ribosomes; however, its mycinose sugar stabilizes U840 in its wild-type position (data not shown).

Discussion

Mutation of G2099A and Its Implication on the Binding of Macrolides

The effect of G2099A mutations on the affinity of *H. marismortui* (Hma) large subunits for erythromycin is of the same order of magnitude, 10^4, as that anticipated on the basis of studies of *E. coli* ribosomes carrying an A to G mutation at that same position (Vester and Douthwaite, 2001). Chemical modification data obtained with *E. coli* indicate that the concentration of erythromycin necessary to protect residues 2058 and 2059 in ribosomes from strains that have a G at position 2058 is also about 10^4 times higher than the concentration required to obtain the same effect in ribosomes from strains that have an A at that position (Douthwaite and Aagaard, 1993).

The reason soak-in experiments done at ligand concentrations below 1 μM provide only upper bound limits for dissociation constants is that the rate at which ligands diffuse into crystals becomes rate limiting at those concentrations and because the total number of ligand molecules in the solutions in which crystals are soaked becomes comparable to the number of drug binding sites in the crystals. Therefore, it is probable that the erythromycin dissociation constant of G2099A large ribosomal subunits from Hma is substantially less than the data presented here appear to document, i.e., <1 μM. Thus, even though we cannot exclude the possibility that the erythromycin dissociation constant of G2099A Hma large subunits might still be 100-fold greater than that reported for *E. coli* ribosomes, ~0.01 μM (Pestka, 1974), the large size of the decrease in dissociation constant the data support gives us confidence that the MLSK antibiotic/Hma large subunit structures reported here are pharmacologically relevant.

Macrolides bind to Hma large ribosomal subunits containing the G2099A mutation almost exactly the same way that they bind to wild-type Hma large subunits. Comparison of the structure of azithromycin bound to wild-type large subunits (Hansen et al., 2002a) with that of the same drug bound to G2099A large subunits (Figure 2F) shows no change in drug orientation or conformation, but only a small –1 Å shift in position. This shift undoubtedly reflects the steric clash that the hydrophilic N2 of G at 2099 in the wild-type particle would have with the drug's C4 methyl group and the middle of its lactone ring if positioned as in the G2099A mutant. If the residue at position 2099 in the erythromycin complex reported here were a G instead of an A, the N2 of G2099 would be only 2.7 Å from C4 methyl of the drug's lactone ring.

While it might seem surprising that the large increase in erythromycin affinity that accompanies the G2099A mutation of Hma large subunit is not accompanied by significant changes in the ways macrolides bind, a similar phenomena has already been observed in HIV re-

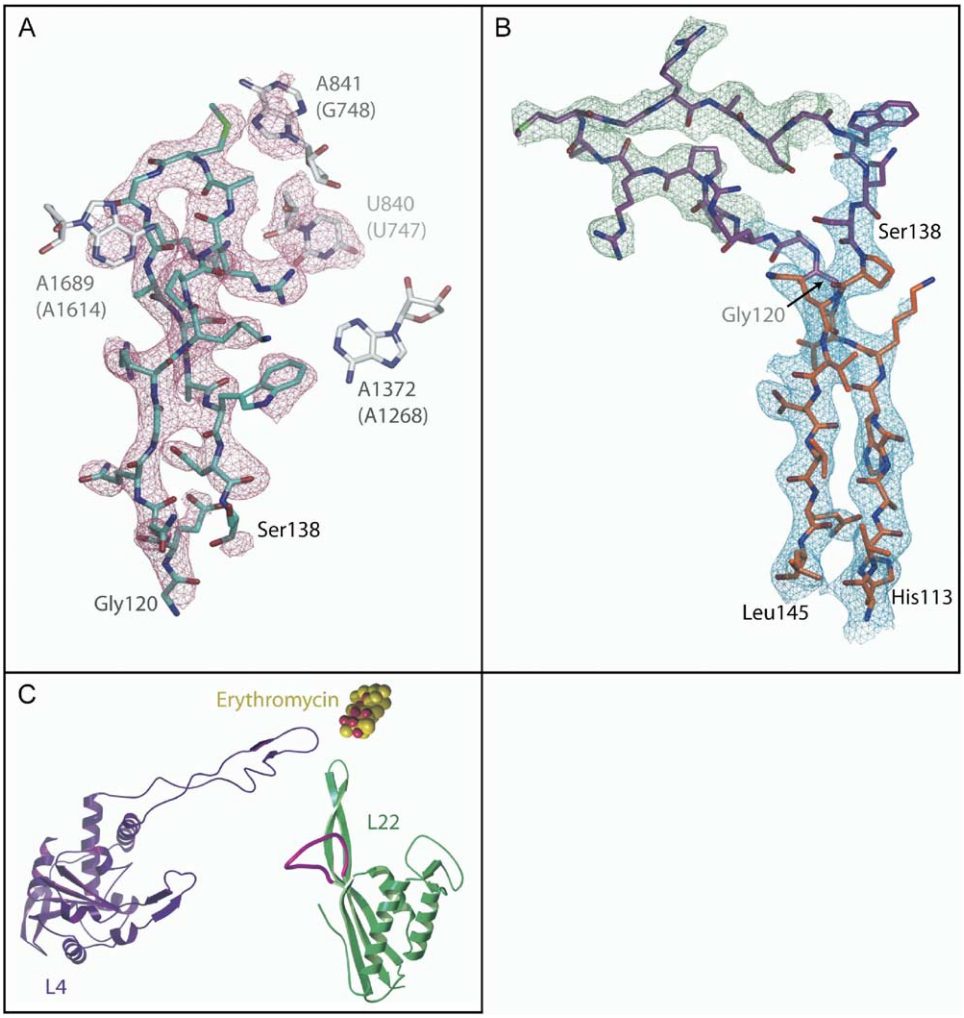

Figure 4. Structure of the Large Subunit Containing the Δ3aa L22 Mutant

(A) A (F_o(L22Δ3aa) – F_o(native)) difference electron density map calculated to a resolution of 2.9 Å and contoured at –6 σ shows that L22's entire C terminus β hairpin has moved away from its native position and several nearby rRNA residues have changed location.

(B) Superposition of a 2.9 Å resolution (F_o(L22Δ3aa) – F_o(native)) difference map (in green) and a (2F_o(L22Δ3aa) – F_o(native)) difference electron density map (in blue) that were contoured at +2.5 σ and +1 σ, respectively, that shows the fading of the 2F_o – F_o density where the loop starts to bend and one of the new loop positions evident in F_o – F_o density.

(C) Schematic showing the relative positions of the L4/L22 gate, the erythromycin binding site, and the movement of L22 β hairpin caused by the Δ3aa mutation.

verse transcriptase (RT) where nonnucleoside inhibitors bind almost identically to resistant mutants of RT and to wild-type RT (Das et al., 1996). In fact, most of the potential for stabilizing interactions between drugs and wild-type targets is preserved in resistance mutants, and binding is often only slightly perturbed.

Telithromycin Binds Tighter Than Erythromycin Because It Makes Additional Interactions with the Ribosome

Telithromycin binds to the ribosome with its lactone ring oriented almost the same as the lactone ring of erythromycin but with its added alkyl-aryl side chain extended above its lactone ring so that it stacks on C2644 (U2609). This additional stacking interaction is consistent with biochemical data obtained in *E. coli* showing that telithromycin binding protects U2609 (*E. coli*) from chemical attack more effectively than erythromycin (Garza-Ramos et al., 2001). This "extra" stacking interaction and the hydrogen bond formed between the nitrogen of pyridine group in telithromycin's aklyl-aryl side chain and the 2′OH of C2644 ribose sugar may also explain why the binding affinity of telithromycin for wild-type bacteria ribosomes is ~10 times higher than that of erythromycin (Hansen et al., 1999). In contrast, this structure does not support the proposal that the enhanced affinity of telithromycin for the ribosome might result from interactions with U845 (A752) (Hansen et al., 1999; Xiong et al., 1999); residue U845 is 6.5 Å from the closest atom of telithromycin.

Virginiamycin: A2103 May Be Critical for Synergy

We have observed a conformational effect that may explain the binding cooperativity of virginiamycin M and

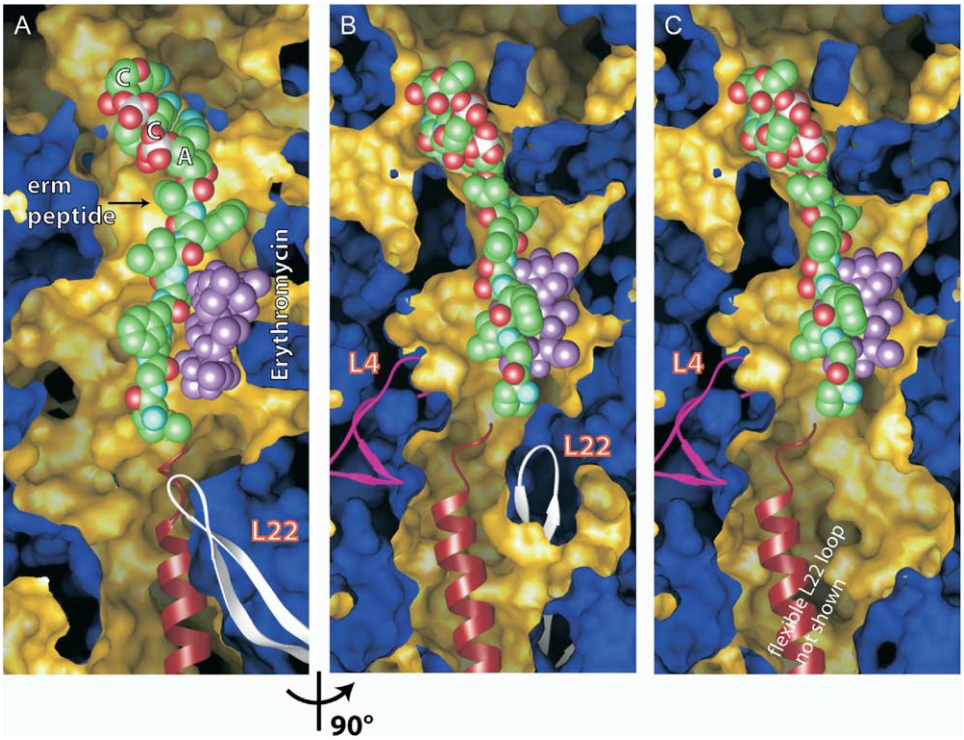

Figure 5. A Model of the Eight N-Terminal Amino Acids of the *ermC* Operon Leader Peptide Bound at the PTC End of the Peptide Exit Tunnel

The molecular surface of the interior of the nascent peptide exit tunnel is shown for the wild-type large ribosomal subunit (A and B) and the L22 deletion mutant ribosome (C). In all three views, it is cut in half along its length to show diameter of the tunnel. In its lower part, polyalanine in α-helical conformation (red) is modeled to mark the general trajectory of the tunnel. Wild-type L22 (white) and L4 (magenta) are shown as ribbons. In (A), the erm peptide (with a sequence of Met-Gly-Ile-Phe-Ser-Ile-Phe-Val) is depicted in a position that would enable it to pass over bound erythromycin (purple) without interfering sterically with either the drug or the surrounding ribosome.

(B) The model in (A) is rotated by 90° to show that by the eighth residue, the peptide has essentially cleared the drug and its N-terminal residue is close to the β hairpin of L22.

(C) In the L22 mutant ribosome, the L4/L22 gate becomes almost twice as wide as it is in the wild-type ribosome as a result of the movement of the β loop of L22. This gives the elongating peptide more room to get past this part of the tunnel, although the wild-type L4/L22 gate does not seem so constricted as to prevent peptide passage even when erythromycin is bound.

S in crystals and their pharmacological synergism. The dissociation constant of vernamycin A (=virginiamycin M) bound to *E. coli* ribosomes is about 1.8×10^{-8} M (Ennis, 1971), and that of virginiamycin S is about 4.0×10^{-7} M (Parfait et al., 1978). However, prior binding of the M component increases the affinity for the S component by about 6-fold (Parfait et al., 1978), but the S compound has no impact on the affinity of the M compound (Cocito and Di Giambattista, 1978). The observation that the M component binds to the wall of peptide tunnel, but the S component binds more in the lumen of the tunnel probably explains why the affinity of virginiamycin M is higher than that of virginiamycin S. The repositioning of A2103 (A2062) that follows the binding of virginiamycin M may well explain their synergy, as suggested previously by Hansen et al. (2003), and more recently by Harms et al. (2004).

The Three Amino Acid Deletion in L22 and Macrolide Resistance

The three amino acid deletion mutation in L22 examined here was originally discovered in *E. coli* strains that are resistant to erythromycin even though their ribosomes still bind erythromycin (Chittum and Champney, 1994; Wittmann et al., 1973). Later, the same deletion mutation was found in *Haemophilus influenzae* strains selected for clarithromycin resistance in vitro (Clark et al., 2002). When the corresponding deletion is made in Hma L22, the entire β hairpin moves away from the tunnel wall and repositions itself further down the tunnel. The electron density for the loop in the mutant suggests that it binds loosely there in several different ways; the refined B factors for this part of L22 are 120 $Å^2$. It seems unlikely that a hairpin so flexibly positioned in the lumen of the peptide exit tunnel would pose a barrier to the passage of nascent peptides through the tunnel.

The relocation of L22 observed in our mutant structure explains almost all of the chemical protection data available which comes from *E. coli*, the organism in which mutations of this type were first isolated. Four of the five residues that have increased chemical reactivities in *E. coli* strains carrying the corresponding L22 mutant (Gregory and Dahlberg, 1999) are located in the immediate vicinity of the region vacated by the β hairpin of L22 in the mutant, and their exposure to solvent is greatly increased. The only residue reported to have an increased chemical reactivity in L22 mutants that is not

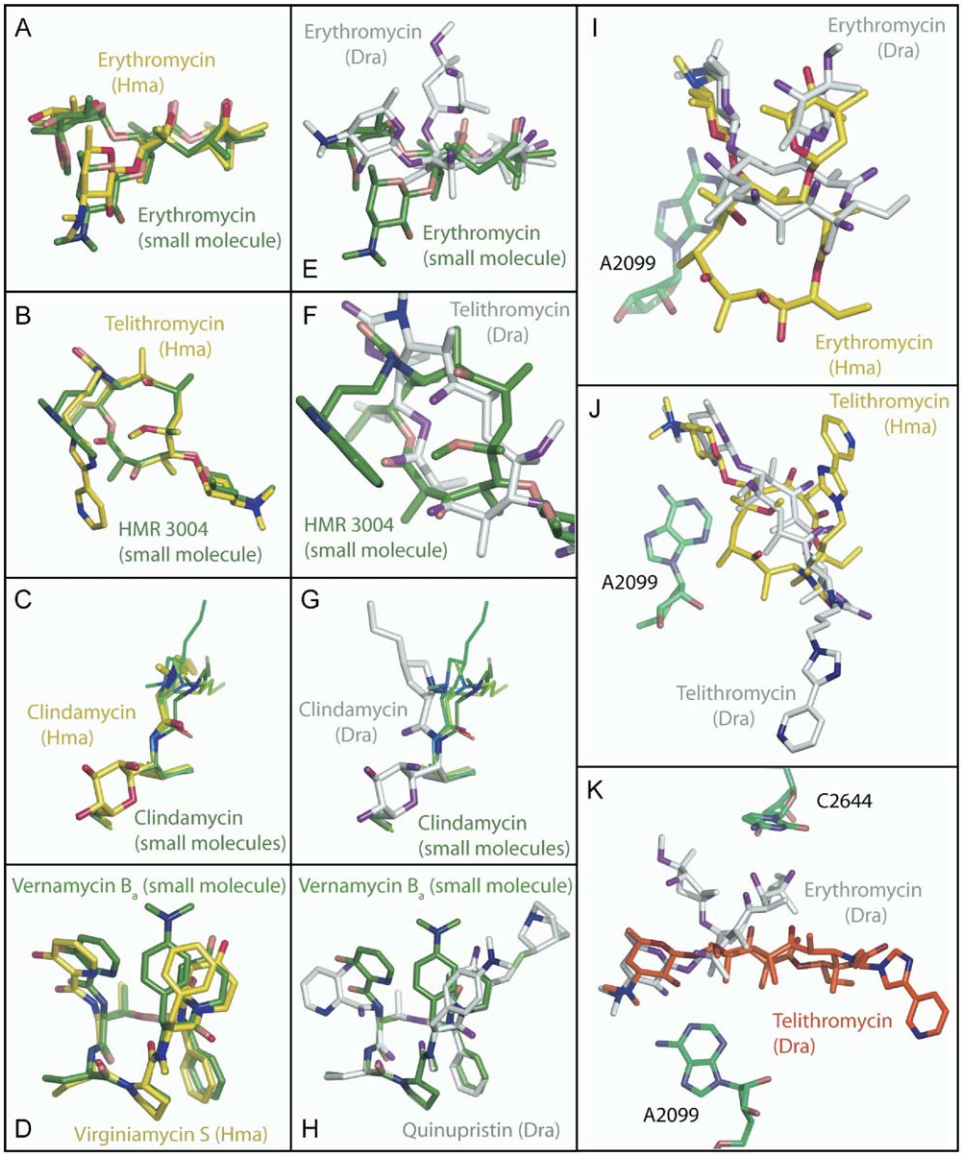

Figure 6. Differences between Models of MLS$_B$K Antibiotics Bound to the *H. marismortui* (Hma) and *D. radiodurans* (Dra) Ribosomes

(A–H) Hma or Dra models of erythromycin, telithromycin, clindamycin, and virginiamycin S are compared to their small molecule crystal structures by least squares alignment of their lactone ring or galactose ring atoms. The conformation of antibiotics bound to Hma ribosomes are all very close to the corresponding small molecule conformations, as can be seen for (A) erythromycin, (B) telithromycin, (C) clindamycin, and (D) virginiamycin S. However, the models for these compounds bound to the Dra large subunit are very different, with erythromycin having its cladinose sugar sticking perpendicular to its lactone ring (E), telithromycin having a highly squashed lactone ring with many atoms unacceptably close together (F), clindamycin's pyrrolidinyl group pointing into a different direction by a peptide bond flip (G), and quinupristin having its conjugated C18 group twisted (H). Aligned by least squares superimposition of rRNA phosphorus atoms, neither the Dra model of erythromycin (I) nor the Dra model of telithromycin (J) fit the corresponding Hma models. In both, the lactone ring of the Dra model tilts away from the hydrophobic binding pocket, and the alkyl-aryl extension of telithromycin goes in a completely different direction.

(K) In the models proposed for erythromycin and telithromycin bound to the Dra ribosome, the lactone rings of the two compounds are tilted relative to each other by about 50°.

close to the β hairpin of L22 is G2385 (G2351), and it is so far away (~90 Å) we are not sure what that observation means. Thus, these correlations give us confidence that the effect of those L22 deletions is the same in Hma as it is in *E. coli*.

The structure of the macrolide binding site in Hma subunits containing the L22 deletion mutation is unaltered, which explains why these mutations do not alter the affinity of the ribosome for macrolides. However, it does not explain why they confer macrolide resistance. In the presence of macrolides, ribosomes synthesize short peptides rather than full-length proteins, and it has long been believed that this results because macrolides prevent the passage of nascent peptides down

the exit tunnel of the large ribosomal subunit. In general, the published structures of complexes between macrolides and the large subunit support this hypothesis. We and others have suggested that the physiological effect of macrolides results from their sterically blocking the lumen of the tunnel (Hansen et al., 2002a), and this may be true for some of them, particularly the larger ones. However, if this were the only mechanism of the macrolide inhibition, then the alteration in the conformation of L22 we observed should have no effect on macrolide phenotype since erythromycin still binds.

Recent biochemical data suggest that the steric block model is incomplete for some macrolides, like erythromycin. Recent data show that erythromycin induces dissociation of peptidyl-tRNAs from the ribosome that carry peptides six, seven, or eight amino acids long, with seven being the dominant length (Tenson et al., 2003). Using the structure of an Hma large ribosomal subunit complex with a P-site substrate (Hansen et al., 2002b) to place the C-terminal residue of peptidyl-tRNAs, we have modeled these peptides into the tunnel of a large subunit of *H. marismortui* with erythromycin bound. The lumen of the tunnel is not so occluded by erythromycin that a peptide cannot get past it (Figures 5A and 5B). Furthermore, the N-terminal residue of an eight residue long peptide would reach a point in the tunnel that is essentially past the drug. It is hard to see why a nascent peptide that has gotten this far down the tunnel should not successfully pass through its entire length. However, we note that just as nascent peptides pass the bound macrolide site, they must negotiate the constriction in the exit tunnel formed by the conjunction of loops of L22 and L4 (Figure 5B), the part of the tunnel altered by the L22 mutations that affect macrolide resistance (Figure 5C). Perhaps, in the presence of erythromycin, it is difficult for nascent peptides to get through this passage.

The structural consequences of this L22 deletion have also been studied by cyroelectron microscopy. Gabashvili and coworkers report that in *E. coli* 70S ribosomes containing the same L22 mutation (Gabashvili et al., 2001), the diameter of the entire upper end of the tunnel increases from ~20 Å to ~26 Å, and they suggest that L22 mutants are resistant to macrolides because the lumen of the tunnel has become so large that it can no longer be obstructed effectively by macrolides. The changes we see are smaller and less extensive. The diameter of the tunnel expands from ~10 Å to ~19 Å but only in the region where L4 and L22 come together in the tunnel. Furthermore, as discussed above, the mechanism of L22 resistance is likely to be more complex, since macrolides bind to the tunnel entirely above the region affected by L22 mutations. Gabashvili et al. also suggested that the rRNA walls of the tunnel become expanded when L22 is mutated this way and speculated that RNA structural changes of this type could conceivably enable the tunnel to function as a peristaltic pump, facilitating the movement of peptide down the tunnel. We see no changes in the backbone positions of the RNA in the mutant and indeed deem changes in the tunnel large enough to propel nascent proteins down it unlikely.

Differences between the Models of MLS_BK Antibiotics Bound to the *H. marismortui* and *D. radiodurans* Ribosomes

The models for MLS_BK antibiotics bound to ribosome that we have presented here and previously (Hansen et al., 2002a) are significantly different from those models provided by the Yonath group (Berisio et al., 2003; Harms et al., 2004; Schlünzen et al., 2001) even though Hma and Dra large subunits have drug binding sites whose sequences are highly conserved. The structural differences between the models fall into three categories: drug conformation, variation in the positions adopted by drugs of the same class when bound to the ribosome, and differences in proposed drug-ribosome interactions. The observations described above indicate that the differences between the models derived for MLS_BK antibiotics bound Hma and Dra large subunit may not necessarily arise from sequence differences between the eubacterial and archaebacterial ribosomes. The G2099A (2058) mutation in the Hma subunit increases its affinity for erythromycin by the same amount (at least 10^4) as the A2058G mutation in the *E. coli* subunit decreases it. Further, the interactions made by erythromycin in the G2099A mutant Hma ribosome should be nearly identical to those it makes in a eubacterial ribosome since the only other base difference in the binding site between the two species affects only a nonsequence-specific stacking interaction.

Crystal structures for most of the antibiotics described here have been previously determined using the pure compound. The conformations of all these antibiotics when bound to the Hma large subunit are almost identical to the conformations they display as isolated compounds. However, the conformations ascribed to these same molecules in their complexes with the Dra large subunit are in many cases very different (Table 2). For example, in both its small molecule crystal structure and in our complex, the cladinose sugar of erythromycin is in its low-energy chair conformation (Stephenson et al., 1997), but in the erythromycin complex with large subunit provided by Schlünzen et al. (2001) it is in the boat conformation. In addition, in the Schlünzen et al. structure, the cladinose sugar is axial relative to the 14-membered lactone ring rather than being equatorial to it, as it is in both our structure and the small molecule crystal structure (Figures 6A and 6E).

In the case of clindamycin, the correspondence between the small molecule crystal structure and the structure of the dug bound to the Hma large subunit is again very close (Figure 6C). Clindamycin consists of a pyrrolidinyl group linked to a galactose sugar by a peptide bond (Figure 1G). In the structure reported by Schlünzen et al. (2001), the relationship between the two rings differs by 180° (*cis* rather than *trans*) from that seen in the small molecule structure (Figure 6G).

There is no small molecule structure for telithromycin, but the structure of its close cousin HMR3004 (Agouridas et al., 1998), which differs only in the nature of the alkyl-aryl group attached to C11/C12 carbamate, reveals that the conformations of the aglycone backbone of 14-membered ketolides and 14-membered macrolides are the same. However, in the telithromycin complex with the large subunit structure of Berisio et al. (2003), the aglycone backbone of the ketolide ring is

Table 2. Comparison of Structures Reported for Antibiotics Bound to Large Ribosomal Subunits with the Structures Available in the Cambridge Structural Database

Antibiotic (CSD[a] number)	*H. marismortui*	*D. radiodurans* (PDB number)
Erythromycin (NAVTAF)	0.745[b]	2.307 (1JZY)
Clindamycin 1[c] (SUPBIO)	0.312	2.100 (1JZX)
Clindamycin 2	1.017	1.868
Clindamycin 3	0.574	2.387
Telithromycin (GOPGAT)	0.260	1.799 (1P9X)
Virginiamycin S (KEFWUN)	0.779	1.733(1SM1)

[a] Cambridge Structural Database.
[b] Root mean square deviations are reported (in Å) for the optimal superposition of the structures being compared. Only atoms common to both the small molecule structures and the antibiotic complex structures reported are aligned and compared.
[c] The different conformations observed for clindamycin 2-phosphate are indicated with numbers.

squashed into a highly elongated form that is very different from the rounded shape it assumes in crystals of pure HMR3004, pure erythromycin, or in any of the structures of the complexes between macrolides and the large subunit that we have obtained (Figures 6B and 6F).

Streptogramin B group compounds are cyclic hexadepsipeptides that contain multiple peptide groups which should be planar due to the partial double bond character of the peptide bond, consistent with the small molecule structure that has been obtained for vernamycin B_{α}, another streptogramin B (Karle and Flippen-Anderson, 1990). This structure shows that the entire [(3-hydroxy-2-pyridinyl)carbonyl] amino group attached to C18 is planar, consistent with its conjugated structure. Nevertheless, in the model proposed by Harms and coworkers for the streptogramin B quinupristin bound to the large subunit (Harms et al., 2004), neither the peptide group nor the 3-hydroxyl of pyridine and the nearby carbonyl group are planar. In addition, the 3-hydroxyl pyridine group turns away from the location it assumes in small molecule structures, and the backbone ring atoms fold together so that the drug no longer looks like a cup (Declercq et al., 1978; Karle and Flippen-Anderson, 1990; Figures 6D and 6H).

While it is certainly possible that the binding of the MLS_BK antibiotics to the Dra ribosome could result in conformational alterations, such distortions would cost free energy, which would decrease their affinities for the ribosome. Thus, the close similarities of the structures of these antibiotics in isolation and bound to the Hma ribosome seem more plausible than the significant changes in their structures reported for the Dra subunit complexes.

The second area of difference between our results and those of Yonath and coworkers is the way drugs of the same chemical class interact with the ribosome. For example, in our models, all macrolides bind very similarly, with the hydrophobic underside of their lactone rings inserted into the hydrophobic cleft formed by residues A2100 (A2059), A2099 (A2058), and G2646 (C2611). In the case of macrolides with the same size lactone rings such as erythromycin and telithromycin, lactone rings superimpose almost perfectly (Figure 2E). This is not the case for the macrolide structures presented by the Yonath group; the lactone rings of these molecules are not modeled in the same location. For example, the orientation of the plane of the lactone ring of erythromycin in their erythromycin complex structure differs from that they observe for telithromycin by about 50° (Figure 6K).

The third area of difference is how the MLS_BK drugs interact with their ribosome target. For example, models of erythromycin or telithromycin bound to the large ribosomal subunits of Dra and Hma posit dramatically different positions for the lactone rings of the macrolides and the alkyl-aryl C11/C12 substituent of the ketolides (Figures 6I and 6J).

Although there are substantial differences between the ways erythromycin is reported to bind to large ribosomal subunits from the two species, the chemical and genetic data in the literature (Vester and Douthwaite, 2001) do not distinguish between them. For example, in *E. coli*, A2059C (*E. coli*) mutations are resistant to macrolides. The authors of the Dra model for the erythromycin complex suggest that a hydrogen bond between the N6 of their A2042 (A2059) and the 2′OH of desosamine sugar explains this observation (Schlünzen et al., 2001). However, the distance between these two atoms is 5.3 Å in their deposited model, while in the Hma subunit complex, the corresponding distance is 4.8 Å. Neither structure easily accounts for this resistance mutation in question. On the other hand, the resistance of ribosomes to dimethylation of A2058 (*E. coli* numbering) or its mutation to G can be rationalized by both structures, since both predict steric clashes that should destabilize macrolide binding. Furthermore, both the Dra and the Hma structures can explain why A2058C and A2058U mutations are resistant to macrolides.

It remains possible that there is a crystallographic explanation for at least some of the differences between the Hma and Dra antibiotic models and the accuracy problems of the published Dra complexes (e.g., in the Dra sparsomycin complex there are no sparsomycin atoms closer than 3.9 Å to a ribosome atom, except two H-bond acceptors that are separated by 3.5 Å [Bashan et al., 2003]). However, since the Dra large subunit models in the PDB lack protein side chains and the observed structure factors for almost none of the complexes reported are available, an independent analysis of this possibility cannot be done.

In conclusion, the comparison of structures of large ribosomal subunits with an A or G in position 2099 (2058) complexed with MLS_BK antibiotics enables us to rationalize how A2058G (*E. coli*) genotype is linked to

the MLS_BK phenotype. In the case of macrolides, ketolides, or streptogramin B class compounds, it is the hydrophilic N2 of G intruding into the hydrophobic face of either the macrolide lactone ring or the C9 benzyl group of virginiamycin S that reduced drug binding. In the case of lincosamides, the change of N6 to O6 upon A to G mutation loosens the extensive hydrogen bond network that clamps the galactose moiety of clindamycin on to the rRNA. Yet another mechanism of resistance is observed in the three amino acid deletion of L22. This deletion in L22 dislodges its β hairpin at the C terminus from its wild-type position into the lumen of the tunnel, widening the gate formed between L4 and L22. There are no changes in the rRNA backbone position, which is consistent neither with an active role for the rRNA in peptide elongation through the tunnel nor with the notation of gross rRNA rearrangements caused by drug-resistance mutations within this ribosomal protein.

Experimental Procedures

The mutant strains of *H. marismortui* were constructed using protocols that are to be published (D.T., G.B., P.B.M., and T.A.S., unpublished data). The purification and crystallization of the large ribosomal subunits from these mutant strains were performed as described previously for the wild-type subunit (Ban et al., 2000). Telithromycin was a generous gift from Aventis Pharma. Virginiamycin was acquired form Research Products International. All other drugs and chemicals were purchased from Sigma. Antibiotics were initially dissolved in dimethyl sulfoxide (DMSO) then added to the standard subunit crystal stabilization buffer (Ban et al., 2000) to yield a final drug concentration of 0.3 μM to 1.0 mM and a DMSO concentration of less than 4%. Crystals were incubated in these stabilization solutions at 4°C for between 8 to 12 hr before being flash-frozen in liquid propane. High-resolution data were collected at beamlines 19ID at APS, 8.2.2. at ALS and ×25 at BNL. Data were reduced using HKL2000 and scaled with SCALEPACK (Otwinowski and Minor, 1997). Models for erythromycin, telithromycin, azithromycin, clindamycin, virginiamycin, and quinupristin and their topology and parameter files were constructed by connecting and/or modifying, if necessary, the related small molecule structures (Agouridas et al., 1998; Karle and Flippen-Anderson, 1990; Kosutic-Hulita et al., 2001; Leban et al., 1994; Stephenson et al., 1997) using standard stereochemical geometry and software, i.e., ChemDraw 3D in combination with XPLO2D (Kleywegt and Jones, 1998) and O (Jones et al., 1991). The antibiotic models were initially fitted into $F_o - F_o$ difference electron density maps, using model phase from the refined crystal structure of the large subunit at 2.4 Å resolution (Klein et al., 2004). The structures of these complexes were refined in an iterative process using CNS (Brünger et al., 1998) for rigid body refinement, energy minimization, and B factor refinement. In all cases, partial occupancies of bound antibiotics were not treated, i.e., they were all set to one. Instead, their refined B factors if high reflect drugs binding only to a fraction of ribosomes in the crystal. Coordinates are available at the Protein Data Bank with accession numbers 1YHQ, 1YI2, 1YIJ, 1YIT, 1YJ9, 1YJN, and 1YJW. Figures were made using ChemDraw, POVScript+ (Fenn et al., 2003), and RIBBONS (Carson, 1997).

Supplemental Data

Supplemental Data include three figures and can be found with this article online at http://www.cell.com/cgi/content/full/121/2/257/DC1/.

Acknowledgments

We thank Larysa Vasylenko for help with preparing 50S ribosomal subunits; Jimin Wang for helpful discussions about crystallographic software; Jeffery Hansen for general support and helpful suggestions during the course of this project; Michael Becker, Robert Sweet, and Lonny Berman for help at BNL; Andres Joachimiak and the staff of ID19 for help at APS; Gerry McDermott and Corie Ralston for help at ALS; and Aventis Pharma for providing telithromycin. The research was supported by National Institutes of Health program grant GM022778 to T.A.S. and P.B.M. and by a grant from the Agouron Institute to T.A.S. and P.B.M.

Received: October 8, 2004
Revised: December 15, 2004
Accepted: February 1, 2005
Published: April 21, 2005

References

Agouridas, C., Denis, A., Auger, J.M., Benedetti, Y., Bonnefoy, A., Bretin, F., Chantot, J.F., Dussarat, A., Fromentin, C., D'Ambrieres, S.G., et al. (1998). Synthesis and antibacterial activity of ketolides (6-O-methyl-3-oxoerythromycin derivatives): a new class of antibacterials highly potent against macrolide-resistant and -susceptible respiratory pathogens. J. Med. Chem. *41*, 4080–4100.

Ban, N., Nissen, P., Hansen, J., Moore, P.B., and Steitz, T.A. (2000). The complete atomic structure of the large ribosomal subunit at 2.4 Å resolution. Science *289*, 905–920.

Bashan, A., Agmon, I., Zarivach, R., Schluenzen, F., Harms, J., Berisio, R., Bartels, H., Franceschi, F., Auerbach, T., Hansen, H.A., et al. (2003). Structural basis of the ribosomal machinery for peptide bond formation, translocation, and nascent chain progression. Mol. Cell *11*, 91–102.

Berisio, R., Harms, J., Schluenzen, F., Zarivach, R., Hansen, H.A., Fucini, P., and Yonath, A. (2003). Structural insight into the antibiotic action of telithromycin against resistant mutants. J. Bacteriol. *185*, 4276–4279.

Brünger, A.T., Adams, P.D., Clore, G.M., DeLano, W.L., Gros, P., Grosse-Kunstleve, R.W., Jiang, J.S., Kuszewski, J., Nilges, M., Pannu, N.S., et al. (1998). Crystallography & NMR system: a new software suite for macromolecular structure determination. Acta Crystallogr. *D54*, 905–921.

Carson, M. (1997). Ribbons. Methods Enzymol. *277*, 493–505.

Chittum, H.S., and Champney, W.S. (1994). Ribosomal protein gene sequence changes in erythromycin-resistant mutants of Escherichia coli. J. Bacteriol. *176*, 6192–6198.

Clark, C., Bozdogan, B., Peric, M., Dewasse, B., Jacobs, M.R., and Appelbaum, P.C. (2002). In vitro selection of resistance in Haemophilus influenzae by amoxicillin-clavulanate, cefpodoxime, cefprozil, azithromycin, and clarithromycin. Antimicrob. Agents Chemother. *46*, 2956–2962.

Cocito, C. (1979). Antibiotics of the virginiamycin family, inhibitors which contain synergistic components. Microbiol. Rev. *43*, 145–192.

Cocito, C., and Di Giambattista, M. (1978). The in vitro binding of virginiamycin M to bacteria ribosomes and ribosomal subunits. Mol. Gen. Genet. *166*, 53–59.

Das, K., Ding, J., Hsiou, Y., Clark, A.D., Jr., Moereels, H., Koymans, L., Andries, K., Pauwels, R., Janssen, P.A., Boyer, P.L., et al. (1996). Crystal structures of 8-Cl and 9-Cl TIBO complexed with wild-type HIV-1 RT and 8-Cl TIBO complexed with the Tyr181Cys HIV-1 RT drug-resistant mutant. J. Mol. Biol. *264*, 1085–1100.

Declercq, J.P., Germain, G., Van Meerssche, M., Hull, S.E., and Irwin, M.J. (1978). Structure cristalline et moléculaire du facteur S de la virginiamycine. Acta Crystallogr. B *34*, 3644–3648.

Douthwaite, S., and Aagaard, C. (1993). Erythromycin binding is reduced in ribosomes with conformational alterations in the 23 S rRNA peptidyl transferase loop. J. Mol. Biol. *232*, 725–731.

Ennis, H.L. (1971). Interaction of vernamycin A with Escherichia coli ribosomes. Biochemistry *10*, 1265–1270.

Fenn, T.D., Ringe, D., and Petsko, G.A. (2003). POVScript+: a program for model and data visualization using persistence of vision ray-tracing. J. Appl. Crystallogr. *36*, 944–947.

Gabashvili, I.S., Gregory, S.T., Valle, M., Grassucci, R., Worbs, M., Wahl, M.C., Dahlberg, A.E., and Frank, J. (2001). The polypeptide tunnel system in the ribosome and its gating in erythromycin resistance mutants of L4 and L22. Mol. Cell *8*, 181–188.

Garza-Ramos, G., Xiong, L., Zhong, P., and Mankin, A. (2001). Binding site of macrolide antibiotics on the ribosome: new resistance mutation identifies a specific interaction of ketolides with rRNA. J. Bacteriol. *183*, 6898–6907.

Gregory, S.T., and Dahlberg, A.E. (1999). Erythromycin resistance mutations in ribosomal proteins L22 and L4 perturb the higher order structure of 23 S ribosomal RNA. J. Mol. Biol. *289*, 827–834.

Hansen, L.H., Mauvais, P., and Douthwaite, S. (1999). The macrolide-ketolide antibiotic binding site is formed by structures in domains II and V of 23S ribosomal RNA. Mol. Microbiol. *31*, 623–631.

Hansen, J.L., Ippolito, J.A., Ban, N., Nissen, P., Moore, P.B., and Steitz, T.A. (2002a). The structures of four macrolide antibiotics bound to the large ribosomal subunit. Mol. Cell *10*, 117–128.

Hansen, J.L., Schmeing, T.M., Moore, P.B., and Steitz, T.A. (2002b). Structural insights into peptide bond formation. Proc. Natl. Acad. Sci. USA *99*, 11670–11675.

Hansen, J.L., Moore, P.B., and Steitz, T.A. (2003). Structures of five antibiotics bound at the peptidyl transferase center of the large ribosomal subunit. J. Mol. Biol. *330*, 1061–1075.

Harms, J.M., Schlunzen, F., Fucini, P., Bartels, H., and Yonath, A. (2004). Alterations at the peptidyl transferase centre of the ribosome induced by the synergistic action of the streptogramins dalfopristin and quinupristin. BMC Biol. *2*, 4.

Jones, T.A., Zou, J.Y., Cowan, S.W., and Kjeldgaard, M. (1991). Improved methods for building protein models in electron-density maps and the location of errors in these models. Acta Crystallogr. *47*, 110–119.

Karle, I.L., and Flippen-Anderson, J.L. (1990). Vernamycin Bα. Acta Crystallogr. C *46*, 303–306.

Klein, D.J., Moore, P.B., and Steitz, T.A. (2004). The roles of ribosomal proteins in the structure assembly, and evolution of the large ribosomal subunit. J. Mol. Biol. *340*, 141–177.

Kleywegt, G.J., and Jones, T.A. (1998). Databases in protein crystallography. Acta Crystallogr. D Biol. Crystallogr. *54*, 1119–1131.

Kosutic-Hulita, N., Matak-Vinkovic, D., Vinkovic, M., Novak, P., Kobrehel, G., and Lazarevski, G. (2001). Conformational behaviour of 11-O-methylazithromycim in the solid and solution state. Croat. Chem. Acta *74*, 327–341.

Krebs, M.P., Mollaaghababa, R., and Khorana, H.G. (1993). Gene replacement in Halobacterium halobium and expression of bacteriorhodopsin mutants. Proc. Natl. Acad. Sci. USA *90*, 1987–1991.

Leban, I., Golic, L., Kotnik, S., Resman, A., and Zmitek, J. (1994). The crystal and molecular structure of the antibiotic clindamycin 2-phosphate hydrate. Acta Chim. Slov. *41*, 405–416.

Malbruny, B., Canu, A., Bozdogan, B., Fantin, B., Zarrouk, V., Dutka-Malen, S., Feger, C., and Leclercq, R. (2002). Resistance to quinupristin-dalfopristin due to mutation of L22 ribosomal protein in Staphylococcus aureus. Antimicrob. Agents Chemother. *46*, 2200–2207.

Otwinowski, Z., and Minor, W. (1997). Processing of X-ray diffraction data collected in oscillation mode. Methods Enzymol. *276*, 307–326.

Parfait, R., de Bethune, M.P., and Cocito, C. (1978). A spectrofluorimetric study of the interaction between virginiamycin S and bacterial ribosomes. Mol. Gen. Genet. *166*, 45–51.

Pestka, S. (1974). Binding of [14C]erythromycin to Escherichia coli ribosomes. Antimicrob. Agents Chemother. *6*, 474–478.

Sanz, J.L., Marin, I., Urena, D., and Amils, R. (1993). Functional-analysis of 7 ribosomal systems from extremely halophilic archaea. Can. J. Microbiol. *39*, 311–317.

Schlünzen, F., Zarivach, R., Harms, J., Bashan, A., Tocilj, A., Albrecht, R., Yonath, A., and Franceschi, F. (2001). Structural basis for the interaction of antibiotics with the peptidyl transferase centre in eubacteria. Nature *413*, 814–821.

Spahn, C.M., and Prescott, C.D. (1996). Throwing a spanner in the works: antibiotics and the translation apparatus. J. Mol. Med. *74*, 423–439.

Stephenson, G.A., Stowell, J.G., Toma, P.H., Pfeiffer, R.R., and Byrn, S.R. (1997). Solid-state investigations of erythromycin A dihydrate: structure, NMR spectroscopy, and hygroscopicity. J. Pharm. Sci. *86*, 1239–1244.

Tenson, T., Lovmar, M., and Ehrenberg, M. (2003). The mechanism of action of macrolides, lincosamides and streptogramin B reveals the nascent peptide exit path in the ribosome. J. Mol. Biol. *330*, 1005–1014.

Vannuffel, P., Di Giambattista, M., and Cocito, C. (1992). The role of rRNA bases in the interaction of peptidyltransferase inhibitors with bacterial ribosomes. J. Biol. Chem. *267*, 16114–16120.

Vester, B., and Douthwaite, S. (2001). Macrolide resistance conferred by base substitutions in 23S rRNA. Antimicrob. Agents Chemother. *45*, 1–12.

Weisblum, B. (1995). Erythromycin resistance by ribosome modification. Antimicrob. Agents Chemother. *39*, 577–585.

Wittmann, H.G., Stoffler, G., Apirion, D., Rosen, L., Tanaka, K., Tamaki, M., Takata, R., Dekio, S., and Otaka, E. (1973). Biochemical and genetic studies on two different types of erythromycin resistant mutants of Escherichia coli with altered ribosomal proteins. Mol. Gen. Genet. *127*, 175–189.

Xiong, L., Shah, S., Mauvais, P., and Mankin, A.S. (1999). A ketolide resistance mutation in domain II of 23S rRNA reveals the proximity of hairpin 35 to the peptidyl transferase centre. Mol. Microbiol. *31*, 633–639.